Beyond quality and quantity: Spatial distribution of contact encodes frictional strength

Sam Dillavou, Yohai Bar-Sinai, Michael P. Brenner, and Shmuel M. Rubinstein, henry location and Astronomy, University of Pennyslvania, Philadelphia, Pennsylvania 19104, USA Pennsylvania and Beverly Sackler School of Physics and Astronomy, Tel Aviv University, Tel Aviv 69978, Israel John A Paulson School of Engineering and Applied Sciences, Harvard University, Cambridge, Massachusetts 02138, USA Google Research, Mountain View, California 94043, USA Racah Institute of Physics, The Hebrew University of Jerusalem, Jerusalem 91904, Israel



(Received 10 March 2022; revised 21 June 2022; accepted 21 July 2022; published 1 September 2022)

Classically, the quantity of contact area A_R between two bodies is considered a proxy for the force of friction. However, bond density across the interface—quality of contact—is also relevant, and contemporary debate often centers around the relative importance of these two factors. In this work, we demonstrate that a third factor, often overlooked, plays a significant role in static frictional strength: The spatial distribution of contact. We perform static friction measurements, μ , on three pairs of solid blocks while imaging the contact plane. By using linear regression on hundreds of image- μ pairs, we are able to predict future friction measurements with three to seven times better accuracy than existing benchmarks, including total quantity of contact area. Our model has no access to quality of contact, and we therefore conclude that a large portion of the interfacial state is encoded in the spatial distribution of contact, rather than its quality or quantity.

DOI: 10.1103/PhysRevE.106.L033001

Static friction, the force required to initiate sliding between two solid bodies, is an illusive quantity that is famously difficult to predict precisely. This reflects the fact that this force is a single scalar which is the outcome of a complex spatiotemporal process of slip nucleation across a typically heterogeneous interface, and as a result depends on a large variety of factors, both controlled [1–10] and uncontrolled (such as wear) [9,10]. Even in well-designed, rigorous laboratory experiments static friction can vary significantly and unpredictably between successive measurements with the same two bodies [9,11]. This stochasticity largely stems from one inconvenient truth about frictional interfaces: Even using the same bulk solids, a new system is formed after each slide. Each such interfacial system contains the ensemble of contact points between two rough bodies, which typically covers a small fraction of the interface due to surface roughness. The frictional strength is classically considered a linear function of the total real contact area of an interface A_R , as the two quantities generally evolve in tandem [1,5,12–16].

Several exceptions to the proportionality between A_R and μ , the static coefficient of friction, were demonstrated recently in the context of frictional aging (strengthening over time) [2,17]. Typically, these works conclude that time-dependent quality of contact—the density of chemical bonding across the interface—explains the discrepancy [18,19]; that is, frictional strength can still be thought of as a function of integrated contact area, albeit appropriately weighted by contact quality. This framework is appealing, as it reduces the relevant state of the entire contact ensemble to a handful of numbers, consistent with the state-of-the-art predictive model for friction, known as rate and state friction laws [20–22]. However, a growing body of evidence suggests that the relevant inter-

facial state is in fact more complex than a single number can describe [8–10,23,24]. Rate and state friction laws are therefore a reasonable but crude approximation of static frictional strength and its details remain the subject of continual debate [25], while the degree of complexity required to model frictional strength is still an open question.

Predicting a single number, such as μ , from a complex data set is a canonical problem in data science. Noteworthy progress has recently been made in predicting laboratory or real earthquakes by utilizing machine learning methods such as convolutional neural networks or boosted decision trees [26–29]. In closely related works, similar methods were used to predict mechanical failure of rocks [30] and amorphous solids [31]. Most work utilizes signals that do not provide direct measurement of the internal interfacial state, meaning that even successful predictions are difficult to interrogate. Some prediction work has been done using direct measurements from bimaterial model faults [29], but with equally complex algorithms, and it is unclear if and how these results may apply to single material, multicontact interfaces. Together, these exciting results indicate that friction is more predictable than previously thought.

Here we use linear regression to predict the static friction coefficient of a multicontact interface undergoing frictional aging using spatially resolved images of its real area of contact and no other inputs. This method is three to seven times more accurate than the benchmark methods of prediction using the total area of contact and experimental parameters. Our results indicate that frictional strength is encoded in the spatial distribution of the real area of contact.

The biaxial compression and translation stage used to measure the friction coefficient is described in detail in a previous

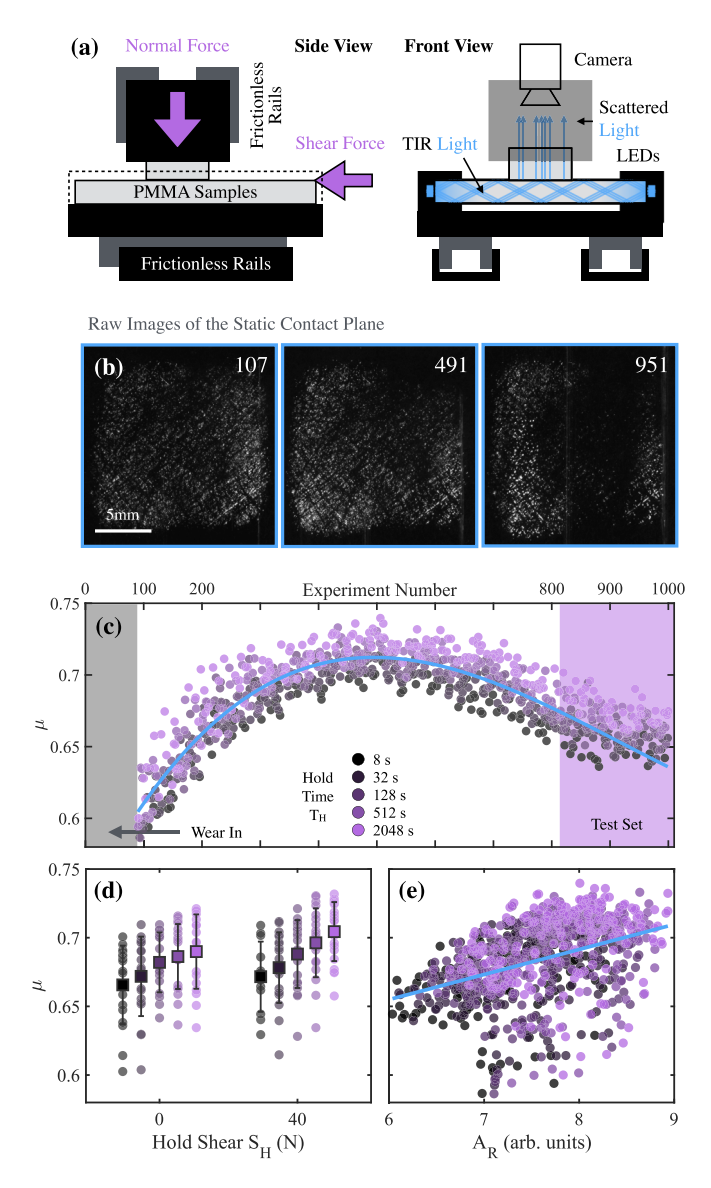


FIG. 1. Experimental setup and benchmark parameters. (a) Left: Schematic of the biaxial compression/translation stage. Right: Embedded optical setup to image the contact ensemble. (b) Three typical images of interfacial contact for after a few dozen, a few hundred, and nearly 1000 experiments, respectively. All data in (b)–(e) is for block pair 1. (c) μ vs experiment number. Colors (shading) in (c)–(e) indicate experimental parameter hold time T_H . The final 18% of data, indicated with shading on the right, is to be used as the test set for predictions. (d) μ for the highest (40 N) and lowest (0 N) hold shears S_H for block pair 1, separated and color (shade) once again represents hold time. Circles are individual experiments, squares are means, and error bars are standard deviations for unique (S_H , T_H) pairs. (e) μ as a function of real area of contact A_R (sum of image intensities). Solid line is a linear fit to all data [cf. (3)].

work [10,23], and shown schematically in Fig. 1(a). Experiments are performed separately on three pairs of laser-cut PMMA (polymethyl-methacrylate) blocks with $1-2.5 \text{ cm}^2$ of nominal contact area. The bottom samples are original, extruded PMMA (11 nm rms), approximately $60 \times 100 \times 4 \text{ mm}$, which are directly contacted by the horizontal force sensor. The top samples are lapped with 1000 grit polishing

paper (~800 nm rms), and are the main source of variance between interfacial systems. While the samples are in contact, the interface is imaged using a total internal reflection (TIR) technique: Single-wavelength (473 nm) light is injected into the bottom sample where it remains trapped though TIR, except at points of actual contact with the top sample. As a result, when imaged from above, the brightness of the interface corresponds to points of real contact, as shown for three examples in Fig. 1(b). The camera position is fixed in relation to the top (smaller, rougher) block, and thus images in subsequent experiments contain common features. Images are grayscale with 8-bit intensity resolution, 5 megapixels, and have a spatial resolution of approximately 1 pixel per 10 μ m, the same order of magnitude as one contact point. Because (summed) pixel intensity is used as our measurement of the real area of contact, this lack of subcontact resolution does not affect our results. This imaging technique is also described in detail in previous work [10].

Static friction measurements are taken via the standard slide-hold-slide protocol: Under constant normal load, $F_N = 90$ N, samples are slid at 0.33 m/s to create a new contact ensemble. The interface is then held static for hold time T_H under constant hold shear force S_H . At the last moment the interface is held static, the image of the contact plane is taken. Subsequently the horizontal motor switches to position control and loads the interface at a rate of 0.33 mm/s (\sim 33 N/s) until the initiation of slip, accompanied by a sharp drop in the measured shear force. We define μ as the highest shear force prior to slip, or the "static peak," divided by the normal load.

Over the course of hundreds of experiments, repeated sliding slowly wears the surfaces of our samples. This effect manifests in changing of the contact ensemble, and generates a slow, and nonmonotonic, drift of the friction coefficient, as shown in Figs. 1(b) and 1(c). This effect is most rapid with a fresh sample, and thus the first several dozen experiments are discarded from our data set ("wear in"). Regardless, to avoid conflating the effect of wear with the effects of changing hold time T_H or hold shear S_H , the experiments are ordered such that every possible combination of experimental variables is performed once in a random order, then again in a different random order and so on. At least five unique values of S_H and of T_H are used for each block (see [32] for details).

Static frictional strength μ has a systematic but noisy dependence on several factors in our data. For example, it is well established that static friction "ages," that is, it is correlated with both the logarithm of the hold time log(t) [1,20,22], and this logarithmic rate is dependent on hold shear S_H [23,33]. Our data shows this expected dependence, as demonstrated in Figs. 1(c) and 1(d). μ is also correlated with real area of contact A_R , as shown in Fig. 1(e). Note that the classical relationships are present in aggregate; A_R , $\log(t)$, and μ are all positively correlated. However, these correlations are swamped by noise, and do relatively little to predict frictional strength for an individual experiment. In previous works with this experimental setup [10,23], wear was treated as a confounding variable, and its resulting slow nonmonotonic trend was subtracted from μ to highlight the effect of experimental parameters. This technique is discussed later in this report as another benchmark outperformed by our method; however, a true prediction of μ should not involve any such

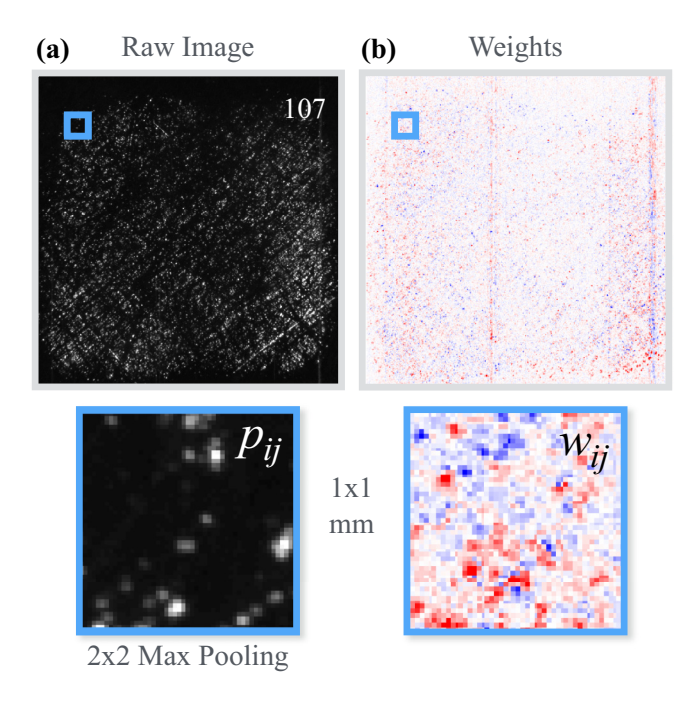


FIG. 2. Image processing and weights. (a) Example raw image (top) from block pair 1, and 1 mm² section (bottom) after 2×2 max pooling. (b) Visualization of the resulting w_{ij} with a zoom in on 1 mm² section from (a). Red is positive, white is zero, and blue is negative.

modification of the data. With or without such detrending, there is a large variance in μ that is not accounted for by experimental parameters and A_R , but, as we show, is in large part predictable from the spatial contact distribution.

We now turn to images of the contact plane to capture this variance. Like most physical (nondigital) systems, our data collection is limited by real-world constraints [34]. Block pairs can be used for only a few hundred to 1000 experiments before they are worn beyond use. Since each image contains millions of pixels ("features"), but each block can only provide $\sim \! 1000$ examples, the problem is massively underconstrained, and we reduce the complexity of our model slightly by square-kernel max pooling by a factor of 4. This reduction speeds computation, and smooths out small-scale details, as shown in Fig. 2(a).

Friction predictions $\hat{\mu}$ are constructed using linear regression of grayscale pixel intensities p_{ij} of these reduced images. Explicitly

$$\hat{\mu}(p_{ij}) = C + \sum_{ij} p_{ij} w_{ij},\tag{1}$$

where C and w_{ij} are fitting parameters (weights) that are constant for each block pair. These are found by standard Ridge regression [35], i.e., a regularized minimization of the prediction error,

$$\underset{w_{ij},C}{\operatorname{argmin}} \left\{ \sum_{n} \left[\mu^{(n)} - \hat{\mu} (p_{ij}^{(n)}) \right]^{2} + \alpha \sum_{ij} w_{ij}^{2} \right\}, \qquad (2)$$

where μ^n and $p_{ij}^{(n)}$ are the static friction coefficient and the interfacial image of the *n*th experiment. α is a hyperparameter

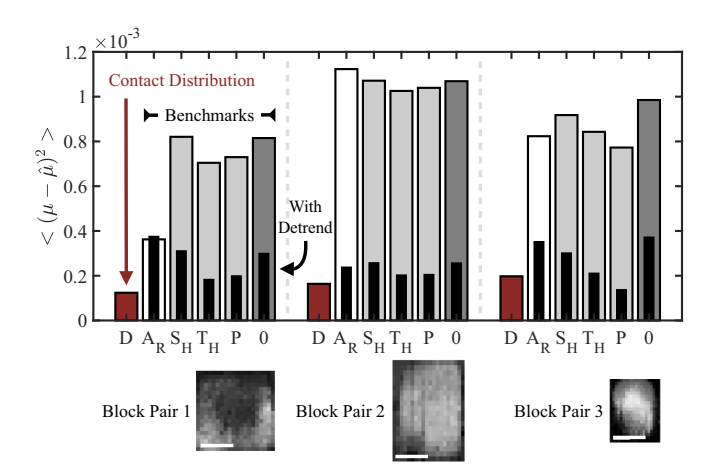


FIG. 3. Contact distribution encodes frictional strength. Test-set mean-squared prediction error for three distinct block pairs. Our linear regression method using the spatial distribution of contact (D) is compared with four methods using global variables. Prediction error for a linear fit to the total area of contact $[A_R, \text{Eq. }(3)]$ is shown in white. The errors of optimal experimental predictors [Eq. (4)] using hold time T_H , hold shear S_H , and both parameters (P) are shown in light gray. Error from predicting the mean value [0, Eq. (5)] is shown in dark gray. Thin black bars indicate error when using these benchmark methods on μ with the slow trend from wear removed as described in text. 10×10 max-pooled example images from each block pair are shown below prediction errors, to scale with one another. Scale bars are 5 mm.

that discourages overfitting. For each block, the first 82% of experiments are used for training and cross validation (i.e., finding the optimal α through leave-one-out cross validation [35]). All metrics reported below are evaluated on the last 18% of the data, which were not used during training. Our model produces w_{ij} that have the size, shape, and granularity of the reduced images, as shown for typical values in Fig. 2(b) for block pair 1. These values are therefore not transferable from pair to pair, as they relate to specific asperities of a single pair. As our interfaces experience irreversible evolution through wear, predicting future values of μ is both more challenging and meaningful than using an interspersed test set; a temporal division of the test set requires w_{ij} to be robust to substantial changes in overall contact distribution, which will inevitably occur in the final 18% of a data set. In contrast, an interspersed train-test split reduces the error of our model, but some of this improvement may be attributed to learning the wear trend, not a true predictive connection between contact distribution and μ . Thus we do not report results obtained in this manner.

Prediction using contact distribution performs strikingly well, as shown in Fig. 3. The most obvious benchmark for comparison is prediction using a linear fit to the *total* contact area A_R ,

$$\hat{\mu}_A(A_R) = a + bA_R, \qquad A_R = \sum_{ij} p_{ij}, \qquad (3)$$

where *a*, *b* are fitting parameters. This gives an error three to seven times higher than our distribution-based predictor. It is worth emphasizing that our regression model is quite distinct from the classical method of aggregating contact area; for our

system, with only a single normal load, we find variations in total A_R to only weakly predict variations in μ . This is likely primarily due to two factors: The lack of any change in normal load, which would generate a larger signal in both friction and A_R , and the substantial change in contact over hundreds of experiments, which generates very distinct interfaces over one sample's lifetime. This is atypical for friction studies, which more often aim to vary normal load and run a much smaller number of experiments on a single sample. However, the fact that our predictions outperform A_R in any regime, even one which is not the most flattering for A_R , suggests that there is information encoded in the spatial contact distribution which is not present in its sum total area.

For completeness, we note that measurement errors might affect the predictive accuracy of A_R as we report it here. However, we expect these effects to be minor. Previous work has shown that the rapid rise in shear force prior to slip (after our images are taken) may modify the contact distribution [6,17,23]. However, this effect would create systematically larger variation for lower hold shear S_H values, which is not the case; we see similar variation in (and covariation between) μ and A_R at all values of S_H , including at constant hold time T_H . This is shown for μ at the highest and lowest values of S_H in Fig. 1(d). It is possible that measurement error in A_R , e.g., from evanescent coupling of interfacial points nearly in contact may also play a role [10], but due to the high number of contact points (thousands) in our system, we expect any such error to be systematic, without large variations between individual experiments, which is not the case.

Another natural benchmark is the optimal predictor that has access to all experimentally controlled parameters. That is, a predictor that predicts the mean friction coefficient conditioned on the protocol,

$$\hat{\mu}_{\text{expt}}(s,t) = \max_{\{s,t\}} \{\mu^{(n)}\},\tag{4}$$

where the mean is taken only over experiments with the specified S_H and T_H . As seen in Fig. 3, $\hat{\mu}_{\text{expt}}$ is only modestly better than predicting the unconditioned mean value,

$$\hat{\mu}_0 = \text{mean}\{\mu^{(n)}\}\tag{5}$$

both generating at least four times higher error than our methods. As previously mentioned, these parameters, along with A_R , do correlate with μ ; however, the signal is drowned in noise for individual experiments, and the relationship between these data and μ may evolve as the interface wears.

It is interesting to ask what the model is and is not learning through regression. Unfortunately, we cannot directly interpret w_{ij} to "understand" the learned interfacial state: The problem is largely overparametrized and therefore there are many different w_{ij} that give similar prediction metrics. For example, using different weight regularization methods, such as LASSO or similar techniques, provides vastly different weights, with comparable predictive power. This makes the weights themselves problematic to interpret directly. Nonetheless, the regression *is* learning aspects of this interfacial system that apply beyond its training set, as seen by the low error on the test set.

Since the weights are not directly interpretable, we must consider the possibility that the model is not learning anything

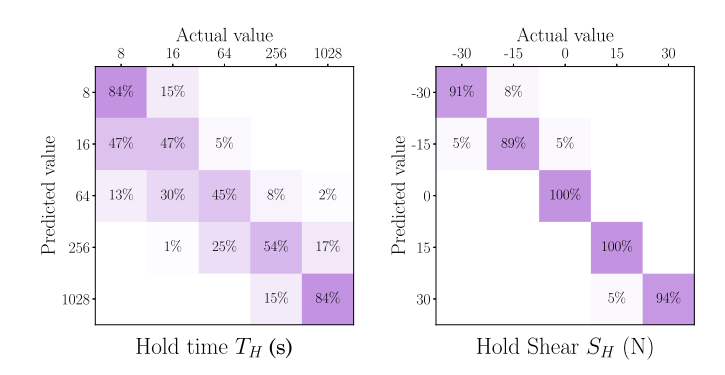


FIG. 4. Experimentally controlled parameters can be extracted from the contact distribution. The percentage of actual and predicted S_H and T_H for block 2. Other blocks show qualitatively similar results

but the connection between μ and the three variables that account for much of its variance, S_H , T_H , and interfacial wear, all of which are encoded in the contact distribution. If this is so, predictions using these three factors should perform at least as well as our model. To give our benchmarks access to the evolution due to wear, we detrend the friction coefficient by defining

$$\tilde{\mu}^{(n)} = \mu^{(n)} - f(n),$$
(6)

where f is a low-order polynomial fit to the training data [different for each block; shown for block pair 1 in Fig. 1(c) as a blue line]. This is similar to methods employed in previous works to increase the signal-to-noise ratio of the evolution of μ as a function of hold time [10,23].

When trained to predict $\tilde{\mu}$ the benchmarks $\hat{\mu}_{\text{expt}}$ and $\hat{\mu}_A$ perform far better than when they are trained to predict μ , as shown by the thin black bars in Fig. 3. However, they are still typically worse than our distribution-based predictor while trained using the raw μ . This suggests the connection between the contact distribution and μ found by our model is not solely mediated by S_H , T_H , and wear. As further evidence, our model is only passable at predicting these experimental parameters. When trained using the same training/test split, but to predict the values of S_H or $\log(T_H)$ instead of μ , our model predicts S_H correctly ± 5 N in 99%, 74%, and 95% of cases, and T_H within a factor of 2 in 62%, 73%, and 100% of cases for block pairs 1, 2, and 3, respectively. The confusion matrix of block 2 is shown in Fig. 4 as a representative example.

Since experiments with the same T_H and S_H follow an identical experimental protocol, the best naive prediction that makes no use of the interfacial state is $\hat{\mu}_{\text{expt}}$, averaged ("trained") on the detrended friction coefficient. Two experiments that are performed with the same protocol with relatively close n are "experimentally identical" and thus variation between them cannot be accounted for with control parameters. With access to interfacial data, however, our model captures some of this variation, outperforming $\hat{\mu}_{\text{expt}}$. Interestingly, unlike the accuracy of the benchmarks, the accuracy of our model does not improve by detrending the data, and in some cases fairs slightly worse, depending on the detrending protocol. This behavior is consistent with the

idea that the contact distribution encodes the raw strength, and therefore predicting the actual μ values is actually easier than learning the detrended $\tilde{\mu}$. To predict a detrended value of the friction coefficient, a model must simultaneously learn a connection to μ and the subtracted trend, which is not trivial to project forward in time.

We have shown that the distribution of interfacial contact encodes information about frictional strength. Using a simple linear model and direct measurements of the real area of contact, we are able to predict future measurements of static friction in an experimental system. These predictions outperform more standard (averaging) predictions using A_R and experimental parameters, and even typically outperform these benchmarks when the overall trend of wear is subtracted from the data.

It is possible that regions given high weight are regions that contain weak contact or high residual stress likely to nucleate slip, or regions that contain "barriers," strong contact regions that stop fledgling slips from propagating to the entire system [36]. We tried several ways to tease out these details. We could not obtain discernible improvements over the linear model by using neural nets, neither terms of error nor explainability (as expected). We also trained predictors using only subsections of the interface, widely varying the size and location of these regions. However, since these problems are so overwhelmingly overparametrized we could not draw any consistent conclusions from the results.

As it stands, our method does not provide a practical mean to model the static friction in real settings. First, it requires both blocks to be transparent and a whole optical apparatus, but more importantly, our regression weights w_{ij} are not

transferable as they are based on the specific details of a data set from a single pair of blocks. However, our results show that the spatial contact distribution can be directly correlated to frictional strength, and that this distribution contains more information than traditional predictions including total quantity of contact. As we cannot measure quality of contact directly, building a quality of contact benchmark is not feasible. However, it is worth emphasizing that our model has no obvious workaround to access to contact quality; pixels in our images even prior to max pooling are on the scale of single contacts, and our model is unable to reliably predict hold time, a factor known to correlate with contact quality. Thus, when our model uses the distribution of contact to eliminate the majority of error produced when using total quantity of contact as a predictor, it implies a strong connection between contact distribution and frictional strength.

It would be interesting to generalize our approach to encode physical knowledge, both in the model and the regularization. In addition, drawing insights from the weights in order to inform coarse-grained friction models going beyond "mean-field" descriptors such as total area, is also a promising avenue for future work.

ACKNOWLEDGMENTS

This research was funded by the National Science Foundation through Division of Mathematical Sciences Grant No. DMS-1715477, MRSEC Grant No. DMR-1420570, ONR Grant No. N00014-17-1-3029, and the Simons Foundation. S.D. acknowledges funding from the Smith Family Fellowship.

- [1] T. Baumberger and C. Caroli, Adv. Phys. 55, 279 (2006).
- [2] Q. Li, T. E. Tullis, D. Goldsby, and R. W. Carpick, Nature (London) 480, 233 (2011).
- [3] L. Bocquet, E. Charlaix, S. Ciliberto, and J. Crassous, Nature (London) 396, 735 (1998).
- [4] M. Nakatani and H. Mochizuki, Geophys. Res. Lett. 23, 869 (1996).
- [5] P. Berthoud, T. Baumberger, C. G'sell, and J.-M. Hiver, Phys. Rev. B 59, 14313 (1999).
- [6] L. Bureau, T. Baumberger, and C. Caroli, Eur. Phys. J E 8, 331 (2002).
- [7] S. L. Karner and C. Marone, Geophysical Monograph Series (American Geophysical Union, Washington, DC, 2000), Vol. 120
- [8] S. L. Karner and C. Marone, Geophys. Res. Lett. 25, 4561 (1998).
- [9] O. Ben-David and J. Fineberg, Phys. Rev. Lett. 106, 254301 (2011).
- [10] S. Dillavou and S. M. Rubinstein, Phys. Rev. Lett. 120, 224101 (2018).
- [11] A. A. Pitenis, D. Dowson, and W. Gregory Sawyer, Tribol. Lett. 56, 509 (2014).
- [12] F. P. Bowden and D. Tabor, *The Friction and Lubrication of Solids* (Clarendon Press, Oxford, 1950).
- [13] J. F. Archard, Proc. R. Soc. A 243, 190 (1957).

- [14] J. A. Greenwood and J. B. P. Williamson, Proc. R. Soc. A 295, 300 (1966).
- [15] B. Persson, J. Chem. Phys. 115, 3840 (2001).
- [16] J. H. Dieterich and B. D. Kilgore, Pure Appl. Geophys. 143, 283 (1994).
- [17] B. Weber, T. Suhina, A. M. Brouwer, and D. Bonn, Sci. Adv. 5, eaav7603 (2019).
- [18] Y. Liu and I. Szlufarska, Phys. Rev. Lett. 109, 186102 (2012).
- [19] K. Tian, N. N. Gosvami, D. L. Goldsby, Y. Liu, I. Szlufarska, and R. W. Carpick, Phys. Rev. Lett. 118, 076103 (2017).
- [20] J. H. Dieterich, J. Geophys. Res. 84, 2161 (1979).
- [21] J. R. Rice and A. Ruina, J. Appl. Mech. 50, 343 (1983).
- [22] A. Ruina, J. Geophys. Res. 88, 10359 (1983).
- [23] S. Dillavou and S. M. Rubinstein, Phys. Rev. Lett. 124, 085502 (2020).
- [24] T. Pilvelait, S. Dillavou, and S. M. Rubinstein, Phys. Rev. Research 2, 012056(R) (2020).
- [25] P. Bhattacharya, A. M. Rubin, and N. M. Beeler, J. Geophys. Res. 122, 6389 (2017).
- [26] B. Rouet-Leduc, C. Hulbert, N. Lubbers, K. Barros, C. J. Humphreys, and P. A. Johnson, Geophys. Res. Lett. 44, 9276 (2017).
- [27] C. Hulbert, B. Rouet-Leduc, P. A. Johnson, C. X. Ren, J. Rivière, D. C. Bolton, and C. Marone, Nat. Geosci. 12, 69 (2019).

- [28] T. Perol, M. Gharbi, and M. Denolle, Sci. Adv. 4, e1700578 (2018).
- [29] F. Corbi, L. Sandri, J. Bedford, F. Funiciello, S. Brizzi, M. Rosenau, and S. Lallemand, Geophys. Res. Lett. 46, 1303 (2019)
- [30] J. McBeck, J. M. Aiken, Y. Ben-Zion, and F. Renard, Earth Planet. Sci. Lett. **543**, 116344 (2020).
- [31] E. D. Cubuk, S. S. Schoenholz, J. M. Rieser, B. D. Malone, J. Rottler, D. J. Durian, E. Kaxiras, and A. J. Liu, Phys. Rev. Lett. 114, 108001 (2015).

- 20, 25, 30, 35, 40}, $T_H = \{16, 32, 64, 128, 256, 512\}$. Block pair 3: $S_H = \{-30, -15, 0, 15, 30\}$, $T_H = \{8, 16, 64, 256, 1024\}$.
- [33] F. Heslot, T. Baumberger, B. Perrin, B. Caroli, and C. Caroli, Phys. Rev. E 49, 4973 (1994).
- [34] J. Hoffmann, Y. Bar-Sinai, L. M. Lee, J. Andrejevic, S. Mishra, S. M. Rubinstein, and C. H. Rycroft, Sci. Adv. 5, eaau6792 (2019).
- [35] C. M. Bishop, Pattern Recognition and Machine Learning (Springer Science, New York, 2006).
- [36] S. Das and K. Aki, J. Geophys. Res. 82, 5658 (1977).